

## Communication

## Ir/Ni Photoredox Dual Catalysis with Heterogeneous Base Enabled by an Oscillatory Plug Flow Photoreactor

Wouter Debrouwer, Wim Kimpe, Ruben Dangreau, Kevin Huvaere, Hannes P. L. Gemoets, Milad Mottaghi, Simon Kuhn, and Koen Van Aken

*Org. Process Res. Dev.*, **Just Accepted Manuscript** • DOI: 10.1021/acs.oprd.0c00150 • Publication Date (Web): 04 Jun 2020

Downloaded from [pubs.acs.org](https://pubs.acs.org) on June 4, 2020

### Just Accepted

“Just Accepted” manuscripts have been peer-reviewed and accepted for publication. They are posted online prior to technical editing, formatting for publication and author proofing. The American Chemical Society provides “Just Accepted” as a service to the research community to expedite the dissemination of scientific material as soon as possible after acceptance. “Just Accepted” manuscripts appear in full in PDF format accompanied by an HTML abstract. “Just Accepted” manuscripts have been fully peer reviewed, but should not be considered the official version of record. They are citable by the Digital Object Identifier (DOI®). “Just Accepted” is an optional service offered to authors. Therefore, the “Just Accepted” Web site may not include all articles that will be published in the journal. After a manuscript is technically edited and formatted, it will be removed from the “Just Accepted” Web site and published as an ASAP article. Note that technical editing may introduce minor changes to the manuscript text and/or graphics which could affect content, and all legal disclaimers and ethical guidelines that apply to the journal pertain. ACS cannot be held responsible for errors or consequences arising from the use of information contained in these “Just Accepted” manuscripts.

1  
2  
3  
4  
5  
6  
7 Ir/Ni Photoredox Dual Catalysis with Heterogeneous  
8  
9  
10  
11 Base Enabled by an Oscillatory Plug Flow  
12  
13  
14  
15 Photoreactor  
16  
17  
18  
19

20 *Wouter Debrouwer,<sup>a\*</sup> Wim Kimpe,<sup>a</sup> Ruben Dangreau,<sup>a</sup> Kevin Huvaere,<sup>a</sup> Hannes P.L. Gemoets,<sup>b</sup>*

21  
22 *Milad Mottaghi,<sup>c</sup> Simon Kuhn,<sup>c</sup> Koen Van Aken<sup>ab</sup>*

23  
24  
25  
26 <sup>a</sup> EcoSynth, Industrielaan 12, 9800 Deinze, Belgium

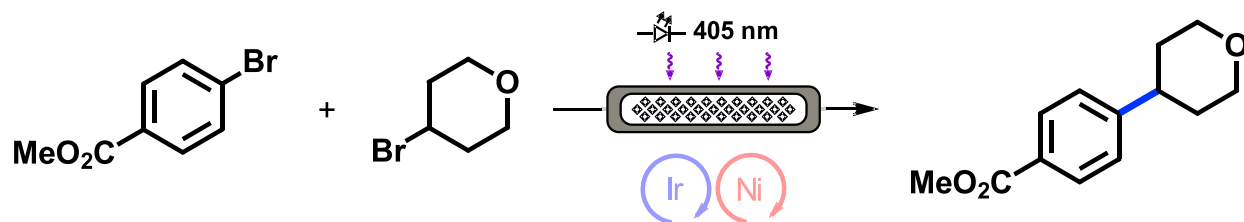
27  
28  
29 <sup>b</sup> Creaflow, Industrielaan 12, 9800 Deinze, Belgium

30  
31  
32 <sup>c</sup> Department of Chemical Engineering, KU Leuven, Celestijnenlaan 200F, 3001, Leuven,  
33  
34  
35 Belgium

36  
37  
38 [wdebrouwer@ecosynth.be](mailto:wdebrouwer@ecosynth.be)

39  
40  
41 **Date received: xx/xx/2020**

## TOC Graphic



- MacMillan metallaphotoredox coupling
- Transfer from milliliter batch to flow procedure
- Inorganic base slurry handling in flow
- Reactor characterization

1  
2  
3 Abstract  
4  
5  
6

7 Continuous flow reactor technology has a proven track record in enabling photochemical  
8 transformations. However, transfer of a photochemical batch process to a flow protocol often  
9 remains elusive, especially when solid reagents or catalysts are employed. In this work, application  
10 of an oscillatory plug flow photoreactor enabled a heterogeneous MacMillan-type  $C(sp^2) - C(sp^3)$   
11 cross-electrophile coupling. Combination of an oscillatory flow regime with static mixing  
12 elements imparts exquisite control over mixing intensity and residence time distribution (RTD),  
13 pinpointing a mindset shift concerning slurry handling in continuous flow reactors. The  $C(sp^2) -$   
14  $C(sp^3)$  cross-electrophile coupling was successfully transferred from batch to flow, resulting in an  
15 intensified slurry process with significantly reduced reaction time and increased productivity (0.87  
16 g/h).  
17  
18  
19  
20  
21  
22  
23  
24  
25  
26  
27  
28  
29  
30

31 Keywords (4-6): HANU reactor, plug flow, oscillatory flow, photoredox catalysis, dual catalysis,  
32 slurry handling  
33  
34  
35  
36  
37  
38  
39  
40  
41  
42  
43  
44  
45  
46  
47  
48  
49  
50  
51  
52  
53  
54  
55  
56  
57  
58  
59  
60

## Introduction

During the past 15 years, the synthetic organic chemist's toolbox has expanded tremendously by the elaboration, control and design of radical-driven transformations. Indeed, access to transient one-electron species has been facilitated thermally,<sup>1</sup> photochemically<sup>2-4</sup> and electrochemically.<sup>5-7</sup> In particular, the amount of reports on photoredox catalysis has grown exponentially since 2010, corroborating widespread adoption in the community.<sup>2</sup> Insights in the underlying chemistry and the ability to access radicals by tuning catalyst photophysical properties have resulted in a myriad of compelling organic transformations.<sup>2-4</sup>

Though empowering those involved in small-scale organic synthesis, photoredox catalysis often proves strenuous when scaling-up. Apart from the usual mass and energy transfer considerations, photon transport to the bulk of the matrix plays a pivotal role.<sup>8</sup> According to Beer-Lambert's law, light attenuation in an absorbing medium follows an exponential decrease.<sup>9</sup> Enlarging reactor dimensions is therefore a poor scale-up strategy, which explains exactly why photochemical transformations strongly benefit from continuous flow reactor technology. The short path length for light penetration (mm range), the high surface-to-volume ratio and the excellent process control outcompete the batch approach.<sup>10-12</sup> Preparative manufacture in flow relies on judicious scale-up of reactor dimensions (i.e. "smart dimensioning"), scale-out or numbering-up.<sup>13-15</sup> Still, continuous flow reactors are often ill-performing when solids handling is concerned, a limiting or even prohibitive factor when envisioning slurry transformations.<sup>11,16-18</sup>

It is the aim of the presented work to demonstrate that such issues can be countered by an innovative plug flow reactor platform, capable of handling solids and particularly apt for photochemistry. This was exemplified by transfer of a heterogeneous MacMillan-type cross-electrophile C(sp<sup>2</sup>) – C(sp<sup>3</sup>) coupling from batch to continuous flow.<sup>19</sup>

## Results and Discussion

### 1) Reactor design

The result of a proprietary design, a flow reactor system that addresses the hurdles commonly encountered upon scaling photochemical transformations was developed.<sup>8,10,12</sup> This concept consists of three major pillars combined: 1) Continuous processing in a linear plate reactor, 2) utilizing an Oscillatory flow regime which is 3) combined with multiple **ST**atic mixing elements in the process channel. These features combined constitute the very essence of the **COSTA** technology (Figure 1), from which a photochemical reactor, the HANU reactor, was conceived. Characteristics and dimensions of the lab-scale reactor are outlined in Table 1.

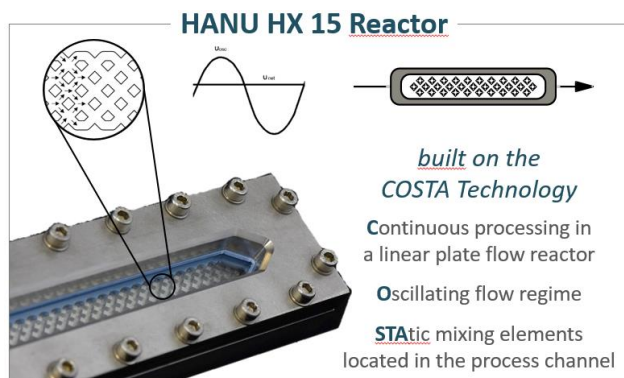


**Figure 1. Principles of the COSTA technology. The COSTA technology consists of 3 pillars: continuous processing in a linear plate reactor by means of an oscillating flow regime and static mixing elements. The oscillating flow regime is characterized by a net flow onto which a periodic flow is superimposed.<sup>20</sup>**

**Table 1. Lab-scale HANU HX 15 reactor characteristics.**

Dimensions	530 x 60 x 45 mm
Reactor volume (irradiated)	15 (14) mL
Window	Borosilicate, Quartz (480 x 17 mm)
Temperature range	-20 °C to + 80°C
Pressure rating	10 barg
Static mixing elements	Cubic (2 x 2 x 2 mm)
Reactor material	Stainless steel 316L or Hastelloy C276
Other wetted parts	FEP, PTFE
Irradiation sources	Mercury lamps, excimers, LEDs

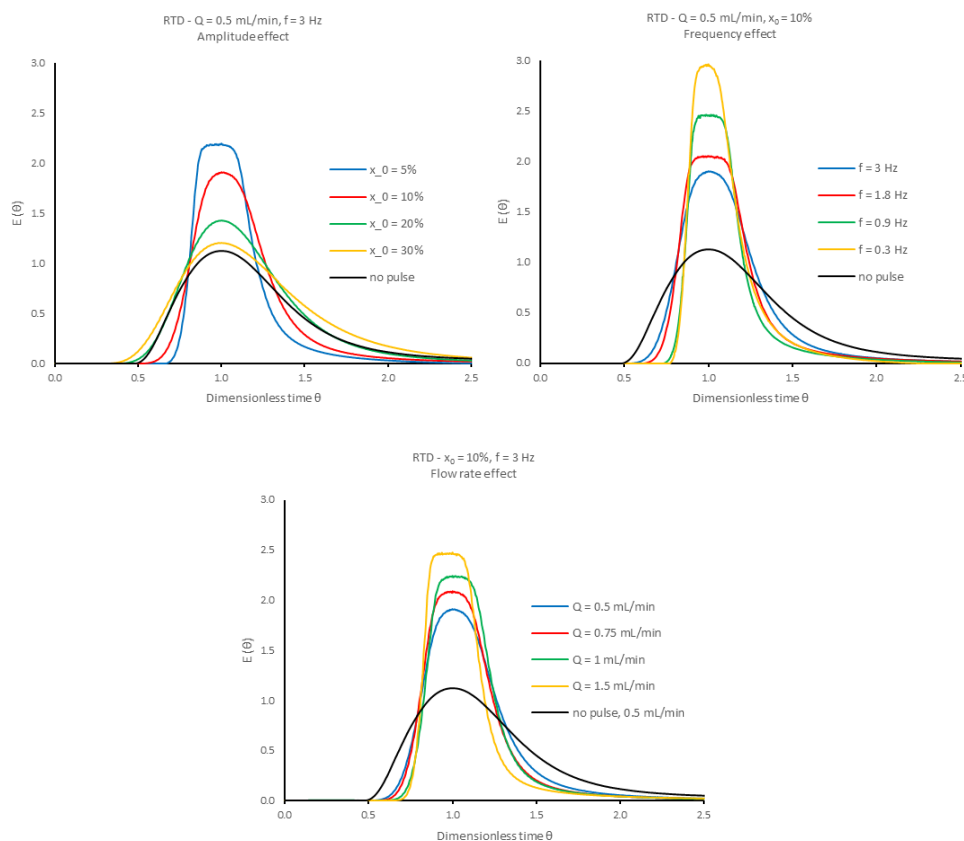
1  
2  
3 The reactor is operated in conjunction with a pulsator, a device that superimposes a periodic  
4 oscillation on the net flow generated by a metering pump.<sup>20-21</sup> This oscillatory flow regime and  
5  
6 repeated split-and-recombine flow path ensure adequate mixing regardless of the net flow rate. In  
7  
8 other terms, reactor hydrodynamics are predominantly decoupled from the net flow rate. As a  
9  
10 consequence, pulsator amplitude and frequency are introduced as new process parameters  
11  
12 affecting hydrodynamics, residence time distribution (RTD), energy dissipation rate and related  
13  
14 transport phenomena, all of which may be optimized on a case-by-case basis. This was exemplified  
15  
16 by the Kappe group utilizing the same reactor to enable C–N coupling with a heterogeneous  
17  
18 catalyst.<sup>22</sup> Depending on process requirements, reactor material, volume and static mixing  
19  
20 elements can be customized.  
21  
22  
23  
24  
25

26 Having determined a set of oscillatory flow parameters, the scale-up principle relies on widening  
27  
28 the process channel without affecting photon path length, mass and energy transfer, and pressure  
29  
30 drop. A “pilot-scale” reactor with 10-fold increased volume was constructed and validated, though  
31  
32 transfer of the C(sp<sup>2</sup>) – C(sp<sup>3</sup>) coupling under investigation here from lab-scale will be the subject  
33  
34 of future work.  
35  
36

## 37 2) RTD

38  
39  
40 As a key parameter in characterizing reactor performance, residence time distributions under  
41  
42 varying conditions were determined. Absorbance curves were recorded by means of tracer  
43  
44 injections (10 mM methylene blue in ethanol) and in-line UV-VIS spectrophotometry at reactor  
45  
46 outlet. Data thus obtained was transformed into E-curves and analyzed using open-open vessel  
47  
48 boundary conditions, after which sloppy tracer input correction was applied.<sup>23</sup> Effect of pulsation  
49  
50 amplitude, frequency and flow rate were on RTD were evaluated (Figure 2). In view of a likely  
51  
52  
53  
54  
55  
56  
57  
58  
59  
60

1  
2  
3 reaction time reduction from 6 h in the corresponding batch process, 30 minutes was tentatively  
4  
5 selected as starting point for the RTD experiments.  
6  
7  
8  
9

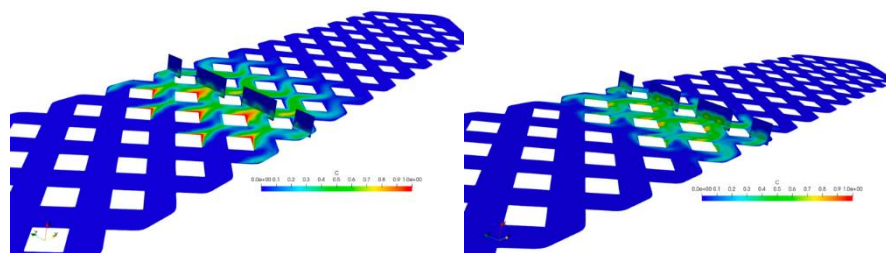


10  
11  
12  
13  
14  
15  
16  
17  
18  
19  
20  
21  
22  
23  
24  
25  
26  
27  
28  
29  
30  
31  
32  
33  
34  
35  
36  
37  
38 **Figure 2. E-curves as function of pulsation amplitude ( $x_0$ , % of maximum pulsation amplitude, 100% corresponds to 7 mm**  
39 **center-to-peak amplitude, top left graph), frequency (top right) and flow rate (bottom).**

40  
41 Higher pulsation amplitudes ( $Q = 0.5$  mL/min,  $f = 3$  Hz) lead to broader RTD, the result of more  
42 axial dispersion. On the other hand, lowering pulsation frequency causes narrowing distributions,  
43 as indeed each additional pulse provokes further axial dispersion. An increased flow rate is  
44 favorable too, although this may be the result of reducing the total amount of pulses. In all cases  
45 pulsed RTD curves are superior to the non-pulsed system, an observation that was confirmed  
46 computationally (see SI). Further optimization by means of statistical methods (including design  
47 of experiment, DOE) would benefit RTD outcome, but is beyond the scope of this work. Moreover,  
48  
49  
50  
51  
52  
53  
54  
55  
56  
57  
58  
59  
60

1  
2  
3 experimental conditions imparting optimal RTD are not necessarily ideal for the specific chemical  
4 reactions under investigation. Slurry handling is pivotal in this work and, while best for RTD, very  
5 low pulsation frequency is counterproductive for maintaining stable suspensions. In reality, finding  
6 the optimal trade-off between RTD and mixing intensity seems best practice.<sup>22</sup>  
7  
8  
9  
10  
11

12 Computational Fluid Dynamic (CFD) simulations support the advantageous effect of pulsation  
13 on RTD (see SI). In addition, by computing tracer transport over time, such simulations allow  
14 comparison of vertical mixing time in absence and presence of pulsation. A drastic increase in  
15 species transport normal to the flow direction is observed with pulsation. The time required for the  
16 scalar species to be transported half the channel height is below 1 s when pulsation is applied,  
17 whereas the tracer did not reach the center of the flow channel within the 7 s of simulation time  
18 (Figure 3).  
19  
20  
21  
22  
23  
24  
25  
26  
27  
28  
29



30  
31  
32  
33  
34  
35  
36  
37 **Figure 3. Concentration field in the reactor  $t = 1.0$  s after tracer injection for a flow rate of 1 ml/min. Left: no pulsation, Right: pulsation frequency of 3 Hz and 33% amplitude.**

### 38 39 3) Actinometry

40  
41  
42 In scientific literature on photoredox catalysis, authors often neglect to quantitatively describe  
43 kinetic parameters and to unambiguously characterize irradiation sources and temperature control  
44 measures. There is growing demand to accurately disseminate on reactor/lamp setup, distance,  
45 emission spectrum and operational parameters.<sup>24</sup> In particular, actinometric data facilitates  
46 reproducibility and quantitative comparison between experimental results.<sup>25-26</sup>  
47  
48  
49  
50  
51  
52  
53  
54  
55  
56  
57  
58  
59  
60

The photoredox catalyst used in MacMillan's work,  $\text{Ir}[\text{dF}(\text{CF}_3)\text{ppy}]_2(\text{dtbbpy})\text{PF}_6$ , displays photon absorption up to ca. 480 nm, with  $\lambda_{\text{max}}$  at 380 nm.<sup>19,27</sup> Use of blue LEDs with multiple emission peaks at 470 nm, 430 nm and 390 nm is reported (34 W Kessil H150b).<sup>19,28</sup> The choice for 405 nm irradiation, available as standard 75 W LED source to mount on the reactor, is thus well justified (irradiation source details are summarized in SI). In order to accurately measure incident photon flux in the reactor, Loubière's chemical actinometry protocol using potassium ferrioxalate was employed.<sup>29,30</sup> For simplicity, the monochromatic irradiation model was adopted (LED emission spectrum half width  $\Delta\lambda = 15$  nm). From ferrioxalate conversion as function of irradiation time (Figure 4), the corresponding photon flux entering the process channel  $q_{n,p}$  was calculated as  $2.96 \times 10^{-5}$  mol photons/s.

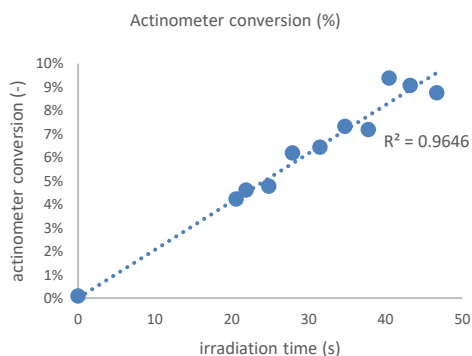


Figure 4. Actinometer conversion as function of irradiation time.

#### 4) Slurry handling

In MacMillan's seminal work, the heterogeneous bases  $\text{K}_2\text{CO}_3$ ,  $\text{Na}_2\text{CO}_3$  and  $\text{LiOH}$  were evaluated and finally  $\text{Na}_2\text{CO}_3$  (2 equiv.) was put forward as most effective for  $\text{C}(\text{sp}^2) - \text{C}(\text{sp}^3)$  cross-electrophile coupling.<sup>19</sup> It performs best with non-heteroaryl substrates whereas heteroaromatic bromides are best combined with anhydrous  $\text{LiOH}$ . In case homogeneous conditions are desired, 2,6-lutidine may replace the inorganic base. However, heterocycles require at least 5 equiv. to reach yields similar to  $\text{LiOH}$ .<sup>31</sup> Taking into account its higher cost (roughly one

1  
2  
3 order of magnitude per mole) and inevitable post-processing removal issues, 2,6-lutidine's  
4 supposed advantages are undone and the choice for Na<sub>2</sub>CO<sub>3</sub> becomes evident, especially during  
5 process development and scale-up.  
6  
7  
8  
9

10 Continuous flow reactor technology creates opportunities for many photochemical reactions, but  
11 the heterogeneous nature of some creates new challenges.<sup>10</sup> Upon translating MacMillan's batch  
12 protocol to flow, the particular difficulty is handling and conveying a Na<sub>2</sub>CO<sub>3</sub> suspension in 1,2-  
13 dimethoxyethane (DME). Typically, plug flow reactors are considered incompatible with solids as  
14 they suffer from plugging and poor solids distribution, while conveying solids requires adequate  
15 pump selection. The integrated HANU concept, on the contrary, anticipates to these issues and  
16 performs exceptionally well in terms of slurry handling. Suspended solids do not sediment because  
17 the oscillatory flow generates high local velocities that constantly resuspend particles and prevent  
18 reactor fouling. Pulsation parameters may be adapted to optimize suspension stability.  
19 Nevertheless, it must be noted that fouling and/or deposition are issues inherently associated with  
20 slurry processing depending on the nature and characteristics of the particles and reactor material,  
21 both in batch and flow. Control and knowledge of slurry physicochemical properties (e.g. particle  
22 size distribution, contact angle, etc.) helps to prevent such issues, and this is the subject of ongoing  
23 research.  
24  
25  
26  
27  
28  
29  
30  
31  
32  
33  
34  
35  
36  
37  
38  
39  
40  
41

42 MacMillan's cross-electrophile coupling thus requires 2 equiv. Na<sub>2</sub>CO<sub>3</sub> in DME, corresponding  
43 to ca. 2.2 wt%.<sup>19</sup> DME is not viscous ( $\mu = 0.46$  mPa.s at 20 °C) with a density of 0.86 kg/L (20  
44 °C), as compared to 2.54 kg/L for Na<sub>2</sub>CO<sub>3</sub>.<sup>32</sup> Stokes' law does not accurately describe particle  
45 sedimentation under conditions prevailing in the reactor, but a similar driving force for settling is  
46 expected and observed accordingly (low solvent viscosity and  $\Delta\rho = 1.68$  kg/L). Preliminary  
47 experiments demonstrated that suspension stability inside the reactor remained excellent due to  
48  
49  
50  
51  
52  
53  
54  
55  
56  
57  
58  
59  
60

the applied oscillations, but issues manifested in supply tubing to the pump. Therefore, investigations continued with the 2.2 wt% Na<sub>2</sub>CO<sub>3</sub> slurry in DME, now in recirculation mode using a peristaltic pump and 0.8 mm ID FEP tubing at different flow rates (Table 2). High flow rates (corresponding to relatively short irradiation times, entries 1-2) proved effective but lower flow rates led to sedimentation of the larger particle fraction in the pump aspiration line. Reduction of the Na<sub>2</sub>CO<sub>3</sub> particle size by wet milling decreased the Sauter mean diameter from 122 μm to 14 μm (see SI for details). The resulting suspensions were maintained in the aspiration line even at very low flow rates, ensuring accurate and precise dosing during reaction.

**Table 2. Impact of flow rate and Na<sub>2</sub>CO<sub>3</sub> particle size on stability of a 2.2 wt% suspension in DME transferred through 0.8 mm inner diameter FEP tubing.**

Entry	d <sub>32</sub> (μm) <sup>a</sup>	Q (mL/min) <sup>b</sup>	τ <sub>irr</sub> (min) <sup>c</sup>	Observations
1	122	5	2.8	Slurry conveyed
2	122	1	14	Slurry conveyed
3	122	0.4	35	Sedimentation in pump supply line
4	14	0.4	35	Slurry conveyed
5	14	0.2	70	Slurry conveyed
6	14	0.1	140	Slurry conveyed

<sup>a</sup> Na<sub>2</sub>CO<sub>3</sub> Sauter mean diameter; <sup>b</sup> flow rate; <sup>c</sup> corresponding irradiation time in the reactor

### 5) Dual Ni/Ir Photoredox cross-electrophile coupling

Having identified conditions that allow conveying the Na<sub>2</sub>CO<sub>3</sub> slurry required for the C(sp<sup>2</sup>) – C(sp<sup>3</sup>) cross-electrophile coupling, the chemical transformation itself was then evaluated. The aim was to present a platform capable of reducing multiple-hour batch reactions to faster and performant flow protocols. A stirred suspension was fed to the integrated photoreactor by means of a peristaltic pump connected to a pulsator in series (Figure 5). The oscillating process stream was exposed to 405 nm irradiation upon entering the reactor channels and left the system through a dome-loaded back-pressure regulator (BPR) after the desired residence time.

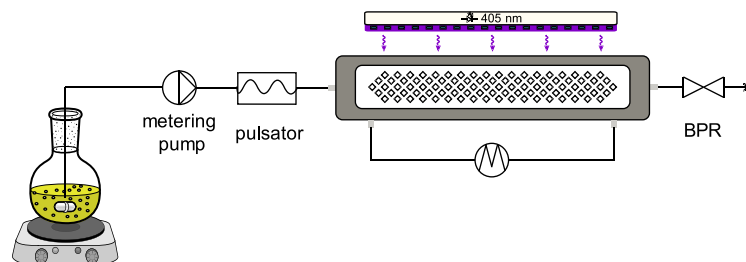


**Figure 5.** Schematic representation of experimental setup used for MacMillan's light-driven cross-electrophile coupling. The  $\text{Na}_2\text{CO}_3$  base remains suspended in the DME reaction solvent by the oscillatory flow regime. The complementary 405 nm LED source covers the entire reactor surface window, thus creating a homogeneous photon flux inside the reaction matrix.

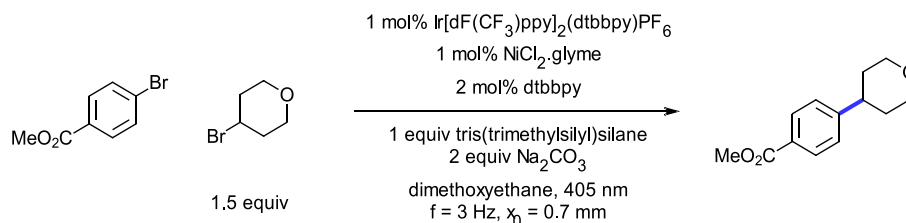
In literature, temperature was maintained at 25 °C by means of convective cooling and no elevated temperatures were assessed. Since the reactor applied here is equipped with an integrated heat exchanger and process thermostat, influence of reaction temperature was readily investigated. Preliminary experiments demonstrate that reaction temperature plays an important role, suggesting the rate-determining step is not photoredox catalyst excitation, but likely a thermal step in the nickel catalyst cycle or a transport phenomenon. The desired reaction proceeds faster at 50 °C without compromising selectivity towards the desired coupled product. To further optimize the thermal component of the catalytic cycle, Ni-loading was doubled to 1 mol% while 2 mol% dtbbpy facilitated catalyst dissolution prior to reaction.<sup>33-34</sup>

We then engaged in a relevant reductive cross-coupling example between methyl 4-bromobenzoate and 4-bromotetrahydropyran. Aiming to maximize productivity, an ambitious 30 minutes of irradiation resulted in complete conversion of the aryl bromide (Table 3). Yield was determined both via  $^1\text{H}$  NMR and isolation of the coupled product, with each method resulting in 76%.<sup>19</sup> As such, yields obtained via  $^1\text{H}$  NMR spectroscopy using internal standard were proven accurate. Observed side products include solvent-coupled methyl benzoate and methyl benzoate.

Further reduction to 20 minutes irradiation furnished an almost identical outcome with substantially increased productivity. Shorter irradiation times (< 20 min) did not lead to full

conversion, suggesting the limits of the system were reached under the prevailing reaction conditions (entries 3-4). Interestingly, further temperature increase to 65 °C improved conversion though selectivity eroded. This was perceived by the unproportionally darker reactor effluent.<sup>35</sup> Considering 50 °C as optimal reaction temperature, irradiation intensity was next halved (entry 6 vs. entry 2). This resulted in only a slight drop in conversion and yield, corroborating the stronger temperature dependence observed earlier. As a final effort to further boost productivity, reactant concentration was increased from 2.3 to 4.2 wt%. An irradiation time of 20 minutes was insufficient but after 30 minutes conversion was complete, culminating in the production of 0.87 g/h of the desired coupled product.

**Table 3. Evaluation of irradiation time, substrate concentration, light intensity, and reaction temperature on conversion and yield of the reductive cross-coupling between methyl 4-bromobenzoate and 4-bromotetrahydropyran, as carried out under continuous flow regime.**



Entry	$\tau^a$ (min)	C <sup>b</sup> (wt%)	Lamp power (%)	T (°C)	Conversion <sup>c</sup> (%)	Yield <sup>d</sup> (%)	Productivity (g/h)
1	30	2.3	100	50	100	76	0.44
2	20	2.3	100	50	100	77	0.71
3	15	2.3	100	50	92	72	0.85
4	10	2.3	100	50	72	61	1.11
5	10	2.3	100	65	80	64	1.12
6	20	2.3	50	50	93	74	0.64
7	20	4.2	100	50	95	79	1.33
8	30	4.2	100	50	100	80	0.87

<sup>a</sup> irradiation time; <sup>b</sup> methyl 4-bromobenzoate concentration; <sup>c</sup> conversion of methyl 4-bromobenzoate as determined by GC-FID analyses using dodecane as internal standard; <sup>d</sup> yield of coupled product as determined by <sup>1</sup>H NMR using mesitylene as internal standard.

1  
2  
3 There are many pitfalls associated with a direct comparison between different photoreactors or  
4 setups. In particular, the incident photon flux is often different due to variations in lamp type,  
5  
6  
7 manufacturer, emitted wavelength, lamp-reactor distance, reactor and light source design, etc.  
8  
9  
10 Table 4 presents an overview of the results obtained for the identical transformation by MacMillan  
11 (batch),<sup>19</sup> Jensen (CSTR-cascade)<sup>36</sup> and in this work. In MacMillan's seminal methodology paper  
12  
13  
14 0.50 mmol methyl 4-bromobenzoate was converted in 6 hours with 79% yield, producing an  
15  
16  
17 average 0.014 g/h of desired product. A 34 W Kessil blue LED was employed. The space-time  
18  
19  
20 yield (STY) was 2.9 g/L/h, though it must be noted that the paper's aim was not productivity  
21  
22  
23 optimization, but methodology development.<sup>19</sup> Jensen's cascade of 5 CSTRs was irradiated by  
24  
25  
26 means of 3 identical 40 W Kessil A160 WE lamps focused onto the reactor window using lenses.  
27  
28  
29 With this setup 0.077 g/h output was realized corresponding to a STY of 14.5 g/L/h.<sup>36</sup> In this work,  
30  
31  
32 finally, 0.87 g/h was produced in an oscillatory plug flow reactor irradiated with quasi-  
33  
34  
35 monochromatic 405 nm LEDs. The STY thus achieved amounts to 62.1 g/L/h, a marked  
36  
37  
38 improvement as compared to the state-of-the-art. The higher incident photon flux per reactor  
39  
40  
41 volume ( $q_{n,p}/V_r$ ) and higher surface-to-volume ratio ( $a_{irr}/V_r$ ) certainly contribute to this  
42  
43  
44 enhancement, highlighting the importance of reactor design, irradiation source power and  
45  
46  
47 integration in the setup. Finally, the photocatalytic space-time yield (PSTY) is a metric that takes  
48  
49  
50 into account both reactor productivity and irradiation source electrical consumption.<sup>37</sup> Though  
51  
52  
53 similar to STY, this value also embodies the efficiency with which lamp input power is translated  
54  
55  
56 into product.  
57  
58  
59  
60

**Table 4. Overview of reaction conditions published for Ir/Ni photoredox C(sp<sup>2</sup>) – C(sp<sup>3</sup>) cross-electrophile coupling of methyl 4-bromobenzoate and 4-bromotetrahydropyran using Na<sub>2</sub>CO<sub>3</sub>.**

Source	C <sup>a</sup> (mM)	V <sub>r</sub> <sup>b</sup> (mL)	τ <sup>c</sup> (h)	T (°C)	P <sup>d</sup> (W)	Productivity (g/h)	STY <sup>e</sup> (g/L/h)	q <sub>n,p</sub> /V <sub>r</sub> <sup>f</sup> (mol/s/m <sup>3</sup> )	a <sub>irr</sub> /V <sub>r</sub> <sup>g</sup> (cm <sup>-1</sup> )	PSTY <sup>h</sup> (g/L/h/W)
MacMillan <sup>19</sup>	10	5	6	25	34 <sup>i</sup>	0.014	2.9	NR	NR	4.21 x 10 <sup>-04</sup>
Jensen <sup>36</sup>	40	5.3	0.5	35	120 <sup>j</sup>	0.077	14.5	0.82 <sup>k</sup>	1.3	6.41 x 10 <sup>-04</sup>
this work	20	14	0.5	50	75 <sup>l</sup>	0.870	62.1	2.12	4.4	1.16 x 10 <sup>-02</sup>

<sup>a</sup> methyl 4-bromobenzoate concentration; <sup>b</sup> reaction volume; <sup>c</sup> irradiation time; <sup>d</sup> lamp input power; <sup>e</sup> space-time yield; <sup>f</sup> incident photon flux (mol photons/s) per reactor volume; <sup>g</sup> reactor irradiated surface-to-volume ratio; <sup>h</sup> photocatalytic space-time yield, defined as the ratio between STY and the standardized lamp power, which is the lamp input power scaled to the power that would irradiate a reactor of 1 L<sup>37</sup>; <sup>i</sup> Kessil blue 34 W LED; <sup>j</sup> 3 x Kessil A160WE 40 W LED; <sup>k</sup> 0.27488 mol/s/m<sup>3</sup> was reported for one lamp based on chemical actinometry (See SI of the reference).<sup>36</sup> This value was multiplied by 3 since 3 lamps were used during reaction.; <sup>l</sup> 405 nm LEDs; NR = not reported.

## Conclusion

The HANU reactor was demonstrated as a continuous plug flow system that is particularly suitable for slurry processing and facilitates transfer of heterogeneous (photochemical) transformations from batch to continuous flow. Several residence time distribution experiments were recorded, assessing the effect of pulsation parameters and flow rate. Incident photon flux was quantified by means of ferrioxalate actinometry and the influence of Na<sub>2</sub>CO<sub>3</sub> particle size on suspension stability was evaluated. The oscillatory flow regime was essential in maintaining stable reactant suspensions. A heterogeneous, milliliter-scale batch Ni/Ir photoredox dual catalyzed transformation was successfully transferred to a plug flow photoreactor. Reaction time was significantly reduced from 6 hours in batch mode to 20 minutes in continuous flow flow, offering perspective for reconsidering the batch approach of a multitude of other (heterogeneous) (photo)chemical reactions.

## Experimental Section

A two-neck 100 mL round bottom flask was equipped with a magnetic stirring bar, photocatalyst Ir[dF(CF<sub>3</sub>)ppy]<sub>2</sub>(dtbbpy)PF<sub>6</sub> (79 mg, 0.07 mmol, 0.01 equiv.), methyl 4-bromo-benzoate (1.505 g, 7.00 mmol, 1.0 equiv.), neopentyl bromide (1.32 mL, 1.586 g, 10.50 mmol, 1.5 equiv.),

1  
2  
3 tris(trimethylsilyl)silane (2.16 mL, 1.741 g, 7.00 mmol, 1.0 equiv.), 28.00 mL of a suspension of  
4  
5 6 wt% Na<sub>2</sub>CO<sub>3</sub> in DME (24.731 g, 1.484 g Na<sub>2</sub>CO<sub>3</sub>, 14.00 mmol, 2.0 equiv.) and 28 mL DME  
6  
7 (23.894 g). The flask was sealed, purged with N<sub>2</sub> and covered in aluminium foil. A separate 25  
8  
9 mL round bottom flask was charged with NiCl<sub>2</sub>·glyme (15 mg, 0.07 mmol, 0.01 equiv.) and 4,4'-  
10  
11 di-tert-butyl-2,2'-bipyridine (38 mg, 0.14 mmol, 0.02 equiv.). The flask was sealed and purged  
12  
13 with N<sub>2</sub>. 14.00 mL DME (12.156 g) was added and the precatalyst solution was sonicated for 5  
14  
15 minutes, after which it was quantitatively transferred into the two-neck reactant flask. The solution  
16  
17 was degassed by sparging with N<sub>2</sub> while stirring for 5 minutes. The stirred suspension was pumped  
18  
19 into the pulsator and reactor using a Vapourtec SF-10 peristaltic pump equipped with blue tube.  
20  
21 Thermostat temperature was set to 50 °C and 2 bar back-pressure was applied. A representative  
22  
23 sample was collected after 3 residence times and analyzed by GC-FID and <sup>1</sup>H NMR spectroscopy.

## 24 25 26 27 28 **Supporting information**

29  
30  
31 The Supporting Information is available free of charge on the ACS Publications website at DOI:  
32  
33 xxx.xxx.

34  
35  
36  
37 The supporting information contains general experimental details, CFD details, irradiation  
38  
39 source characteristics, particle size distributions and compound characterization data.

## 40 41 42 **Corresponding Author**

43  
44  
45 \*Wouter Debrouwer (wdebrouwer@ecosynth.be)

## 46 47 48 **Author Contributions**

49  
50  
51 The manuscript was written through contributions of all authors. All authors have given approval  
52  
53 to the final version of the manuscript.

## ACKNOWLEDGMENT

Financial support from Vlaio (Flanders Innovation and Entrepreneurship) is gratefully acknowledged (HBC.2019.2081). We thank Bert Metten and Sophie Nols (Ajinomoto Bio-Pharma Services) for wet milling of Na<sub>2</sub>CO<sub>3</sub>.

## ABBREVIATIONS

a <sub>irr</sub>	irradiated reactor surface [cm <sup>2</sup> ]
BPR	back-pressure regulator
C	concentration [wt %]
CFD	computational fluid dynamic
CSTR	continuous stirred tank reactor
DME	1,2-dimethoxyethane
DOE	Design of Experiments
d <sub>32</sub>	Sauter mean diameter [μm]
f	frequency [Hz]
FEP	fluorinated ethylene propylene
ID	inner diameter [mm]
LED	light-emitting diode
P	lamp power [W]

PTFE	polytetrafluoroethylene
Q	flow rate [mL/min]
$q_{n,p}$	photon flux [mol photons/s]
RTD	residence time distribution
T	temperature [°C]
UV-VIS	ultraviolet – visible light
$V_r$	reactor volume [mL]
$x_0$	center-to-peak amplitude [% of maximum or mm]
$\mu$	dynamic viscosity [mPa.s]
$\rho$	density [kg/L]
$\tau_{irr}$	irradiation time [min]

## REFERENCES

- [1] Smith, J.M.; Dixon, J.A.; deGruyter, J.N.; Baran, P.S. Alkyl Sulfinates: Radical Precursors Enabling Drug Discovery, *J. Med. Chem.* **2019**, *62*, 2256-2264.
- [2] Shaw, M.H.; Twilton, J.; MacMillan, D.W.C. Photoredox Catalysis in Organic Chemistry, *J. Org. Chem.* **2016**, *81*, 6898-6926.
- [3] Romero, N.A.; Nicewicz, D.A. Organic Photoredox Catalysis, *Chem. Rev.* **2016**, *116*, 10075-10166.

- 1  
2  
3 [4] Prier, C.K.; Rankic, D.A.; MacMillan, D.W.C. Visible Light Photoredox Catalysis  
4 with Transition Metal Complexes: Applications in Organic Synthesis, *Chem. Rev.* **2013**, *113*,  
5 5322-5363.  
6  
7  
8  
9  
10 [5] Echeverria, P.-G; Delbrayelle, D.; Letort, A.; Nomertin, F.; Perez, M.; Petit, L. The  
11 Spectacular Resurgence of Electrochemical Redox Reactions in Organic Synthesis, *Aldrichimica*  
12 *Acta* **2018**, *51*, 3-19  
13  
14  
15  
16 [6] Wiebe, A.; Gieshoff, T.; Möhle, S.; Rodrigo, E.; Zirbes, M.; Waldvogel, S.R.  
17 Electrifying Organic Synthesis, *Angew. Chem. Int. Ed.* **2018**, *57*, 5594-5619.  
18  
19  
20  
21 [7] Yan, M.; Kawamata, Y.; Baran, P.S. Synthetic Organic Electrochemical Methods  
22 Since 2000: On the Verge of a Renaissance, *Chem. Rev.* **2017**, *117*, 13230-13319.  
23  
24  
25  
26 [8] Aillet, T.; Loubière, K.; Prat, L.; Dechy-Cabaret, O. Impact of the Diffusion  
27 Limitation in Microphotoreactors, *AIChE* **2015**, *61*, 1284-1299.  
28  
29  
30  
31 [9] Harper, K.C.; Moschetta, E.G.; Bordawekar, S.V.; Wittenberger, S.J. A Laser  
32 Driven Flow Chemistry Platform for Scaling Photochemical Reactions with Visible Light, *ACS*  
33 *Cent. Sci.* **2019**, *5*, 109-115.  
34  
35  
36  
37 [10] Cambié, D.; Bottecchia, C.; Straathof, N.J.W.; Hessel, V.; Noël, T. Applications of  
38 Continuous-Flow Photochemistry in Organic Synthesis, Material Science, and Water Treatment,  
39 *Chem. Rev.* **2016**, *116*, 10276-10341.  
40  
41  
42  
43  
44 [11] Plutschack, M.B.; Pieber, B.; Gilmore, K.; Seeberger, P.H. The Hitchhiker's Guide  
45 to Flow Chemistry, *Chem. Rev.* **2017**, *117*, 11796-11893.  
46  
47  
48  
49 [12] Loubière, K.; Oelgemöller, M.; Aillet, T.; Dechy-Cabaret, O.; Prat, L.  
50 Continuous-flow photochemistry: A need for chemical engineering, *Chem. Eng. Proc.* **2016**, *104*,  
51 120-132.  
52  
53  
54  
55  
56  
57  
58  
59  
60

1  
2  
3 [13] Yayla, H.G.; Peng, F.; Mangion, I.K.; McLaughlin, M.; Campeau, L.-C.; Davies,  
4 I.W.; DiRocco, D.A.; Knowles, R.R. Discovery and mechanistic study of a photocatalytic indoline  
5  
6  
7  
8  
9  
10  
11  
12  
13  
14  
15  
16  
17  
18  
19  
20  
21  
22  
23  
24  
25  
26  
27  
28  
29  
30  
31  
32  
33  
34  
35  
36  
37  
38  
39  
40  
41  
42  
43  
44  
45  
46  
47  
48  
49  
50  
51  
52  
53  
54  
55  
56  
57  
58  
59  
60

dehydrogenation for the synthesis of elbasvir, *Chem. Sci.* **2016**, *7*, 2066-2073.

[14] Noël, T.; Gelonch, M.E.; Huvaere, K. Industrial Photochemistry: From Laboratory  
Scale to Industrial Scale, In *Photochemical processes in continuous flow reactors*; Noël, T., Ed.;  
World Scientific: Europe, **2017**; pp 245-267.

[15] Berton, M.; de Souza, J.M.; Abdiaj, I.; McQuade, D.T.; Snead, D.R. Scaling  
continuous API synthesis from milligram to kilogram: extending the enabling benefits of micro to  
the plant *J. Flow Chem.* **2020**, *10*, 73-92.

[16] For an example where a heterogeneous base, LiOH, was substituted prior to transfer  
from batch to flow requiring extra screening efforts, see: Brill, Z.G.; Ritts, C.B.; Mansoor, U.F.;  
Sciammetta, N. Continuous Flow Enables Metallaphotoredox Catalysis in a Medicinal Chemistry  
Setting: Accelerated Optimization and Library Execution of a Reductive Coupling between  
Benzylic Chlorides and Aryl Bromides, *Org. Lett.* **2020**, *22*, 410-416.

[17] For an example where a heterogeneous base, e.g. Cs<sub>2</sub>CO<sub>3</sub>, was substituted prior to  
transfer from batch to flow requiring extra screening efforts, see: Hsieh, H.-W.; Coley, C.W.;  
Baumgartner, L.M.; Jensen, K.F.; Robinson, R.I. Photoredox Iridium–Nickel Dual-Catalyzed  
Decarboxylative Arylation Cross-Coupling: From Batch to Continuous Flow via Self-Optimizing  
Segmented Flow Reactor, *Org. Process Res. Dev.* **2018**, *22*, 542-550.

[18] Mo, Y.; Jensen, K.F. A miniature CSTR cascade for continuous flow of reactions  
containing solids, *React. Chem. Eng.* **2016**, *1*, 501-507.

- 1  
2  
3 [19] Zhang, P.; Le, C.; MacMillan, D.W.C. Silyl Radical Activation of Alkyl Halides in  
4 Metallaphotoredox Catalysis: A Unique Pathway for Cross-Electrophile Coupling, *J. Am. Chem.*  
5 *Soc.* **2016**, *138*, 8084-8087.  
6  
7  
8  
9  
10 [20] Mongeon, S.S.; Roberge, D.M.; Bittel, M.; Elsner, P.; Macchi, A. Liquid–Liquid  
11 Mass Transfer in an Oscillatory-Flow Mesoscale Coil Reactor without Baffles, *Org. Process Res.*  
12 *Dev.* **2016**, *20*, 733-741.  
13  
14  
15  
16  
17 [21] Doyle, B.J.; Gutmann, B.; Bittel, M.; Hubler, T.; Macchi, A.; Roberge, D.M.  
18 Handling of Solids and Flow Characterization in a Baffleless Oscillatory Flow Coil Reactor, *Ind.*  
19 *Eng. Chem. Res.* **2020**, *59*, 4007–4019.  
20  
21  
22  
23  
24 [22] Rosso, C.; Gisbertz, S.; Williams, J.D.; Gemoets, H.P.L.; Debrouwer, W.; Pieber,  
25 B.; Kappe, C.O. An oscillatory plug flow photoreactor facilitates semi-heterogeneous dual  
26 nickel/carbon nitride photocatalytic C–N couplings, *React. Chem. Eng.* **2020**, *5*, 597-604.  
27  
28  
29  
30  
31 [23] Fogler, H.S. Elements of Chemical Reaction Engineering, 5<sup>th</sup> ed.; Prentice Hall,  
32 2016.  
33  
34  
35  
36 [24] Bonfield, H.E.; Knauber, T.; Lévesque, F.; Moschetta, E.G.; Susanne, F.; Edwards,  
37 L.J. Photons as a 21st century reagent, *Nat. Commun.* **2020**, *11*, 804.  
38  
39  
40  
41 [25] Ziegenbalg, D.; Wriedt, B.; Kreisel, G.; Kralisch, D. Investigation of Photon Fluxes  
42 within Microstructured Photoreactors Revealing Great Optimization Potentials, *Chem. Eng.*  
43 *Technol.* **2016**, *39*, 123-134.  
44  
45  
46  
47 [26] Corcoran, E.B.; McMullen, J.P.; Lévesque, F.; Wismer, M.K.; Naber, J.R. Photon  
48 Equivalents as a Parameter for Scaling Photoredox Reactions in Flow: Translation of  
49 Photocatalytic C-N Cross- Coupling from Lab Scale to Multikilogram Scale, *Angew. Chem. Int.*  
50 *Ed.* **2020**, DOI: 10.1002/anie.201915412.  
51  
52  
53  
54  
55  
56  
57  
58  
59  
60

1  
2  
3 [27] Lowry, M.S.; Goldsmith, J.I.; Slinker, J.D.; Rohl, R.; Pascal, R.A.; Malliaras, G.G.;  
4  
5 Bernhard, S. Single-Layer Electroluminescent Devices and Photoinduced Hydrogen Production  
6  
7 from an Ionic Iridium(III) Complex, *Chem. Mater.* **2005**, *17*, 5712-5719.

8  
9  
10 [28] For a representative emission spectrum of Kessil lamps, see: Bonfield, H.E.;  
11  
12 Mercer, K.; Diaz-Rodriguez, A.; Cook, G.C.; McKay B.S.J.; Slade, P.; Taylor, G.M.; Ooi, W.X.;  
13  
14 Williams, J.D.; Roberts, J.P.M.; Murphy, J.A.; Schmermund, L.; Kroutil, W.; Mielke, T.;  
15  
16 Cartwright, J.; Grogan, G.; Edwards, L.J. The Right Light: De Novo Design of a Robust Modular  
17  
18 Photochemical Reactor for Optimum Batch and Flow Chemistry, *ChemPhotoChem* **2020**, *4*, 45-  
19  
20 51.

21  
22  
23 [29] Aillet, T.; Loubiere, K.; Dechy-Cabaret, O.; Prat, L. Accurate Measurement of the  
24  
25 Photon Flux Received Inside Two Continuous Flow Microphotoreactors by Actinometry *Int. J.*  
26  
27 *Chem. React. Eng.* **2014**, *12*, 1-13.

28  
29  
30 [30] Wriedt, B.; Ziegenbalg, D. Common pitfalls in chemical actinometry, *J. Flow*  
31  
32 *Chem.* **2020**, *10*, 295-306.

33  
34  
35 [31] For a number of tips and tricks and extra information related to base selection, see:  
36  
37 [http://chemlabs.princeton.edu/macmillan/reactions/silyl-radical-mediated-metallaphotoredox-](http://chemlabs.princeton.edu/macmillan/reactions/silyl-radical-mediated-metallaphotoredox-cross-electrophile-coupling/)  
38  
39 [cross-electrophile-coupling/](http://chemlabs.princeton.edu/macmillan/reactions/silyl-radical-mediated-metallaphotoredox-cross-electrophile-coupling/), accessed on March 26, 2020.

40  
41  
42 [32] CRC Handbook of Chemistry and Physics, 87<sup>th</sup> edition; Lide, D.R., Ed.; CRC Press:  
43  
44 Boca Raton, 2006.

45  
46  
47 [33] Ting, S.I.; Garakyaraghi, S.; Taliaferro, C.M.; Shields, B.J.; Scholes, G.D.;  
48  
49 Castellano, F.X.; Doyle, A.G. <sup>3</sup>d-d Excited States of Ni(II) Complexes Relevant to Photoredox  
50  
51 Catalysis: Spectroscopic Identification and Mechanistic Implications, *J. Am. Chem. Soc.* **2020**,  
52  
53 *142*, 5800-5810.

1  
2  
3 [34] Beromi, M.M.; Brudvig, G.W.; Hazari, N.; Lant, H.M.C.; Mercado, B.Q. Synthesis  
4 and Reactivity of Paramagnetic Nickel Polypyridyl Complexes Relevant to C(sp<sup>2</sup>)-C(sp<sup>3</sup>)  
5 Coupling Reactions, *Angew. Chem. Int. Ed.* **2019**, *58*, 6094-6098.  
6  
7

8  
9  
10 [35] For a report on nickel-black formation and concomitant reaction mixture color  
11 change, see: Gisbertz, S.; Reischauer, S.; Pieber, B. Overcoming Limitations in Dual  
12 Photoredox/Nickel catalyzed C-N Cross-Couplings due to Catalyst Deactivation, ChemRxiv  
13 Preprint, <https://doi.org/10.26434/chemrxiv.10298735.v1>  
14  
15  
16  
17

18  
19 [36] Pomberger, A.; Mo, Y.; Nandiwale, K.Y.; Schultz, V.L.; Duvadie, R.; Robinson,  
20 R.; Altinoglu, E.I.; Jensen, K.F. A Continuous Stirred-Tank Reactor (CSTR) Cascade for Handling  
21 Solid-Containing Photochemical Reactions, *Org. Process Res. Dev.* **2019**, *23*, 2699-2706.  
22  
23  
24

25  
26 [37] Leblebici, M.E.; Stefanidis, G.D.; Van Gerven, T. Comparison of photocatalytic  
27 space-time yields of 12 reactor designs for wastewater treatment, *Chem. Eng. Proc.* **2015**, *97*, 106-  
28  
29  
30  
31  
32  
33  
34  
35  
36  
37  
38  
39  
40  
41  
42  
43  
44  
45  
46  
47  
48  
49  
50  
51  
52  
53  
54  
55  
56  
57  
58  
59  
60